*International Journal of Advanced Geosciences*, 14 (1) (2026) 43-54

International Journal of Advanced Geosciences

*Website: www.sciencepubco.com/index.php/IJAG*
*https://doi.org/10.14419/p29jqd76*
***Research paper***

# Petrography, Geochemistry, and Lithium Exploration Potential of Pan-African Granitoids from Pamsi Area (Northern Cameroon Domain)

**Amadou Diguim Kepnamou [1] *, Naïmou Seguem [2], Ganwa Alembert Alexandre [3, 4], Noussi Fossi William Luther [3], Ntoumbé Mama [3], Haskandi Kalaza Josue [3]**

*[1] Department of Earth Science and Environment, Faculty of Sciences, University of Garoua, P.O Box 346, Garoua, Cameroon*
*[2] Department of Life and Earth Science, University of Moundou, Moundou, Chad*
*[3] Department of Mining Geology, School of Geology and Mining Engineering, University of Ngaoundere, P.O Box 115, Meiganga, Cameroon*
*[4] Department of Earth Science, Faculty of Sciences, University of Ngaoundere, P. O Box 454, Garoua, Cameroon*
**Corresponding author E-mail: amadoudiguim@yahoo.fr*

*Received: February 19, 2026, Accepted: April 17, 2026, Published: April 21, 2026*

**Abstract**

This study presents an integrated petrographic and geochemical investigation of granitoid and metamorphic rocks from the Pamsi locality in the North Cameroon Domain of the Pan-African Fold Belt. Field observations, microscopic analysis, and whole-rock geochemistry reveal five main lithological units: amphibole-biotite granite, leucogranite, granodiorite, orthogneiss, and amphibolite. These rocks form a calc-alkaline suite ranging from syeno-diorite to granite, classified as I-type, sub-alkaline, potassic to hyperpotassic, and predominantly peraluminous to metaluminous. Geochemical signatures include strong LREE enrichment, negative Eu anomalies in most samples, and multi-element patterns showing negative Ta-Nb, Sr, and Ti anomalies with positive Th, Zr, and U anomalies, characteristic of differentiated magmas from mixed crustal-mantle sources. Tectonic discrimination diagrams indicate volcanic arc to syn-collisional settings consistent with Pan-African orogenesis. Pathfinder element analyses reveal preliminary indications of lithium exploration potential, with samples N11 and N51 showing notable cesium enrichment (8.80–11.30 ppm) and elevated Cs/Rb ratios. Based on established geochemical correlations—and pending direct lithium measurements—estimated lithium contents of 200–800 ppm are proposed as preliminary targets for further investigation. These results highlight the Pamsi area as a promising prospect for lithium mineralization associated with evolved pegmatitic systems, warranting systematic follow-up studies.

***Keywords***: *Petrology; Geochemistry; Lithium Exploration; Pan-African Fold Belt; North Cameroon Domain; Pamsi.*

## 1. Introduction

Lithium has emerged as a critical metal in the global transition toward renewable energy and electric mobility, with demand projected to increase exponentially in the coming decades [1]. While traditional lithium sources have been concentrated in South America and Australia, recent exploration efforts have shifted toward identifying new lithium-bearing provinces, particularly within granite-pegmatite systems associated with evolved magmatic complexes [2], [3]. In Central Africa, the Pan-African orogenic belt presents significant potential for hosting lithium mineralization, yet systematic geochemical and petrological investigations remain limited.

The North Cameroon Domain, part of the Central African Pan-African chain (Fig. 1), is characterized by extensive Neoproterozoic to Cambrian magmatism that includes calc-alkaline granitoids, post-tectonic granites, and associated pegmatite systems [4], [5]. These magmatic suites, formed during various stages of continental collision and crustal reworking, exhibit geochemical signatures indicative of evolved melts with potential for rare metal enrichment. Despite growing interest in the metallogenic potential of this region, comprehensive studies integrating field observations, petrographic analysis, and whole-rock geochemistry to assess lithium prospectivity remain scarce.

The Pamsi locality, situated within the North Cameroon Domain, exposes a variety of granitoid rocks whose petrogenesis and metallogenic significance have not been previously investigated. Understanding the geochemical evolution and crystallization history of these rocks is essential for evaluating their potential to host lithium mineralization, particularly in pegmatitic phases associated with highly fractionated granitic melts.

This study presents the first integrated petrographic and geochemical investigation of the Pamsi granitoids and associated metamorphic rocks. The objectives are to: (1) characterize the petrographic features and mineral assemblages of the main rock types; (2) determine their geochemical signatures and magmatic evolution; (3) establish their geodynamic setting within the Pan-African orogeny; and (4) assess

their preliminary lithium mineralization potential based on pathfinder element associations. The results contribute to a better understanding of the metallogenic framework of the North Cameroon Domain and provide preliminary exploration targets for future lithium prospecting in the region.

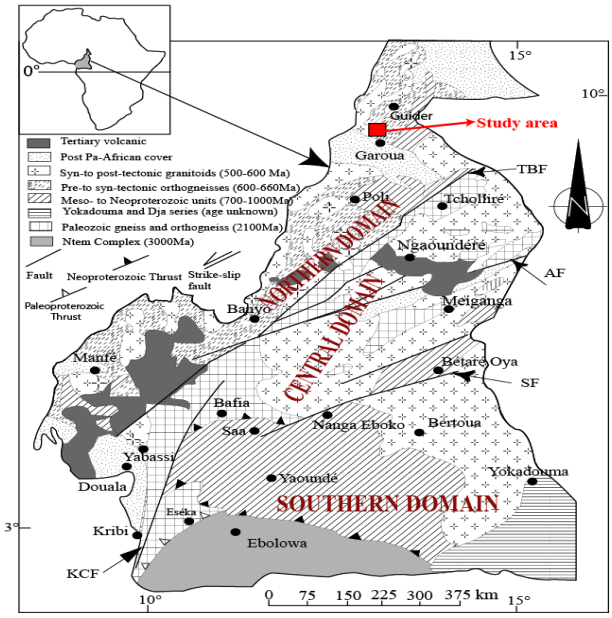


**Fig. 1:** Geological Map of the Pan-African Fold Belt (PAFB) of the North Congo Craton Showing the Study Area (Simplified After [4]).

## 2. Geological Setting

The study area (Fig. 2) belongs to the North Cameroon Domain, also referred to as the North-West Cameroon Domain [4, 5] in relation to its location northwest of the Tcholliré-Banyo fault (and continuing into neighboring Nigeria). To the south and southwest, it is separated from the Central Cameroon Domain by the Tcholliré-Banyo fault, and to the east, it is connected to the Mayo Kebbi Domain. Its western boundary remains unclear. This part of the Pan-African chain has been the subject of several research works, including those of [6 -11]. The basement is covered by metasediments and metavolcanics of Upper Proterozoic age (830 Ma, U/Pb on zircon). Calc-alkaline granitoids dated at 530 Ma and post-tectonic granites of alkaline composition are also found in this domain [12]. Structurally, three phases of deformation—D1, D2, and D3—have been identified [12 - 14].

The D1 phase is characterized by tangential tectonics responsible for early planar (S1), linear (L1), and folded (P1) structures. The D2 phase corresponds to sinistral N-S or WSW-ENE strike-slip faults. The D3 phase is marked by E-W-trending shear zones generally associated with E-W or N-S axis drag folds. Previous work conducted in this domain allows the distinction of five geological units: (1) the Poli group (schists and gneisses with a significant Neoproterozoic juvenile component and a minor Paleoproterozoic contribution, without any Archean material [15], [16]); (2) pre- to syn-tectonic granitoids (metadiorites and metagranodiorites); (3) syn- to late-tectonic granitoids (medium-grained to porphyroid granites with pink alkali feldspar); (4) post-tectonic granitoids (leucogranites and syenites); and (5) molassic depositional basins (e.g., the Mangbaï series). These geological units are intruded by alkaline granites, syenites, and Tertiary-age mafic dykes, and are sometimes covered by plateau alkaline basalts.

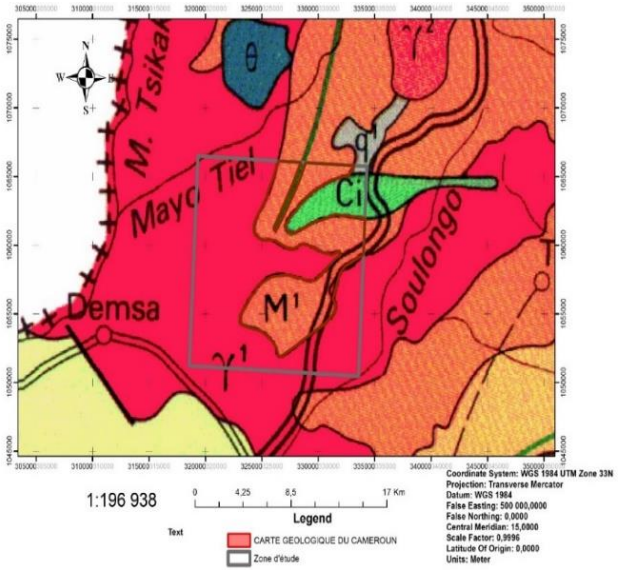


**Fig. 2:** Geological Map of Pamsi Locality.

# 3. Materials and Methods

## 3.1. Petrography

The petrographic investigation began with field-scale observations, which allowed for the macroscopic identification of the various granitoid facies and their constituent minerals. Representative samples were collected from outcrops across the Pamsi area. Thin sections were prepared at the Department of Earth Sciences, Faculty of Sciences, University of Yaoundé I, Cameroon. Petrographic examinations were conducted using a polarizing microscope to determine mineralogical compositions, textural relationships, and alteration features of the different granitoid types.

## 3.2. Geochemistry

Geochemical analyses were performed on seven representative samples from each granitoid type identified in the field. While this sample size is modest, samples were selected to ensure coverage of all five identified lithological units across the accessible outcrop exposures. The samples were crushed, pulverized, and analyzed for major, trace, and rare earth elements at ACME Analytical Laboratories (Vancouver, Canada) using ICP-AES (Inductively Coupled Plasma-Atomic Emission Spectroscopy) and ICP-MS (Inductively Coupled Plasma-Mass Spectrometry) techniques.

Sample preparation followed the alkaline fusion method, where 200 mg of each powdered sample was mixed with 900 mg of lithium metaborate ($LiBO_2$) flux. The mixture was then fused and dissolved in a nitric acid ($HNO_3$) solution. Major elements were determined by ICP-AES and reported as weight percent oxides, while trace and rare earth elements were determined by ICP-MS and reported in parts per million (ppm). Quality control procedures included the analysis of certified reference materials, duplicates, and blanks. Analytical precision was better than ±2% for major elements, ±5% for trace elements with concentrations >10 ppm, and ±10% for trace elements with concentrations <10 ppm.

It should be noted that lithium was not directly measured in this study. Lithium potential is assessed indirectly through pathfinder elements (notably Cs, Rb, Ta, and U), and all lithium estimates presented herein are preliminary and require validation through direct analysis.

# 4. Results

## 4.1. Petrographic study

Field investigations and petrographic analyses reveal that the rocks in the Pamsi area comprise five main types: amphibole-biotite granite, leucogranite, granodiorite, orthogneiss, and amphibolite (Fig. 3).

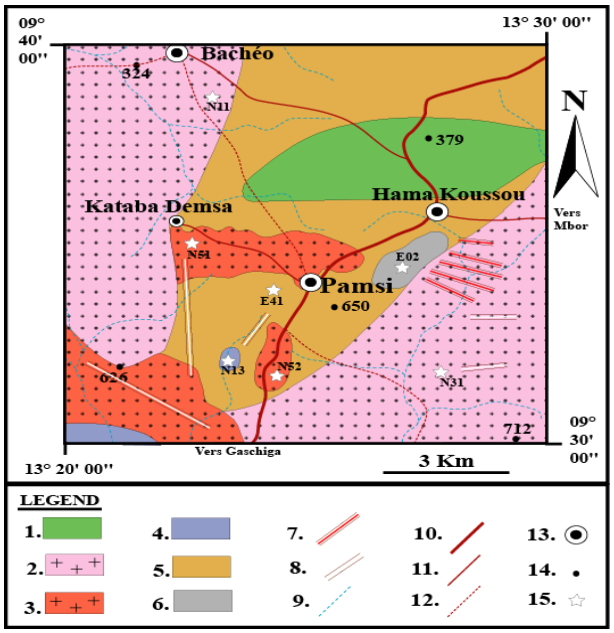


**Fig. 3:** Sampling Map of Pamsi Region. 1. Sandstone; 2. Leucogranite; 3. Amphibole and Biotite Granite; 4. Granodiorite; 5. Orthogneiss; 6. Amphibolite; 7. Aplite Dyke; 8. Quartz Dyke; 9. Hydrography; 10. Main Road; 11. Secondary Road; 12. Track; 13. Locality: 14. Side Point; 15. Sample.

### 4.1.1. Amphibole-biotite granite

Under the microscope, the amphibole-biotite granite exhibits a granular texture (Figs. 4a and 4b). It is composed of amphibole, biotite, quartz, plagioclase, orthoclase, chlorite, and opaque minerals. Amphibole is a green hornblende in subhedral to anhedral crystals averaging approximately 1 mm, constituting about 10% of the rock volume. It contains inclusions of quartz and opaque minerals (Fig. 4a). Biotite (approximately 10%) forms dark brown flakes 0.5–1.5 mm long, associated with amphibole and opaque minerals. Quartz represents 25% of the rock volume, forming subhedral to anhedral crystals of variable size (0.2–1.5 mm) with undulatory extinction. Orthoclase (approximately 20%) forms elongated, sometimes perthitic crystals 2–3 mm long. Plagioclase (approximately 20%) forms euhedral to subhedral crystals averaging 1.5 mm in length, recognized by polysynthetic twins tapering to a wedge shape at the mineral edge (Fig. 4c). Opaque minerals (approximately 5%) occur as inclusions in amphibole, biotite, and feldspars.

### 4.1.2. Leucogranite

The leucogranite exhibits a granular texture at thin section scale (Fig. 4d) and is composed of amphibole, biotite, quartz, plagioclase, orthoclase, microcline, and opaque minerals. Amphibole (approximately 5%) is a green hornblende ranging from 0.1 to 0.5 mm. Biotite (10%) forms dark brown flakes averaging 0.25 mm, containing quartz inclusions. Quartz (30%) forms patches of variable size (0.1–0.8 mm) with undulatory extinction. Plagioclase (20%) forms subhedral, albite-twinned crystals averaging 1 mm, containing submicroscopic opaque inclusions and partially replaced by sericite. Orthoclase (20%) and microcline (10%) form subhedral crystals of comparable size to plagioclase; the latter is recognized by cross-hatched (tartan) twins with myrmekite buds at its margins (Fig. 4f). Opaque minerals (5%) occur as inclusions in amphibole and plagioclase.

### 4.1.3. Granodiorite

The granodiorite has a granular texture (Figs. 4g and 4h) and is composed of amphibole, biotite, quartz, plagioclase, orthoclase, microcline, chlorite, and opaque minerals. Amphibole (20%) is a green hornblende with crystals ranging from 1–3 mm. Biotite (25%) forms brown flakes of 0.5–2 mm, locally altered to chlorite. Quartz (10%) occurs as subhedral to anhedral grains averaging 0.5 mm. Plagioclase (25%) forms subhedral crystals with well-developed albite twins (Fig. 4i). Orthoclase (20%) and microcline (15%) form subhedral crystals of 1–2 mm with opaque mineral inclusions. Opaque minerals (5%) are found as inclusions in all major mineral phases.

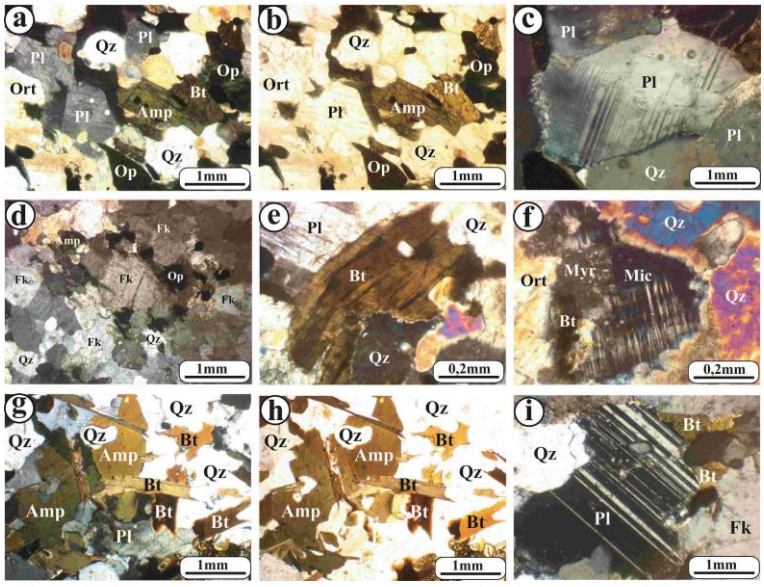


**Fig. 4:** Photomicrography of Plutonic Rock Thin Sections. A) Granular Texture of Amphibole-Biotite Granite (XPL); B) Granular Texture of Amphibole-Biotite Granite (PPL); C) Plagioclase with Wedge-Shaped Twin Termination (XPL); D) Granular Texture of Leucogranite (XPL); E) Biotite Flake with Quartz Crystal Inclusion (XPL); F) Microcline with Myrmekite Bud Development at Its Margin (XPL); G) Granular Texture of Granodiorite (XPL); H) Granular Texture of Granodiorite (PPL); I) Plagioclase Crystal with Albite Twins (XPL).

### 4.1.4. Orthogneiss

The orthogneiss shows a granoblastic texture with a tendency toward grano-lepidoblastic texture (Fig. 5a), composed of biotite, quartz, plagioclase, orthoclase, chlorite, apatite, and opaque minerals. Biotite (approximately 25%) occurs in flakes grouped in discontinuous beds, defining the rock's foliation, and is locally transformed into chlorite. Quartz (approximately 35%) forms polycrystalline patches and ribbons, averaging approximately 1.5 mm, with undulatory extinction. Plagioclase (approximately 25%) forms subhedral patches of 0.5–1.5 mm. Orthoclase (approximately 10%) is perthitic with vein-like quartz exsolutions (Fig. 5c). Accessory minerals include chlorite (approximately 3%), apatite (approximately 2%), and opaque minerals (approximately 10%).

### 4.1.5. Amphibolite

The amphibolite has a granoblastic texture (Figs. 5d and 5e) and is composed of amphibole (approximately 60%), biotite (approximately 5%), quartz (approximately 10%), plagioclase (approximately 8%), orthoclase (approximately 7%), and opaque minerals (approximately 10%). Amphibole is a green hornblende reaching up to 3 mm in length, containing inclusions of quartz and opaque minerals (Fig. 5e). Biotite forms very fine flakes and is locally altered to chlorite. Quartz forms parallel polycrystalline ribbons in places. Opaque minerals occur as inclusions in biotite and quartz (Fig. 5f).

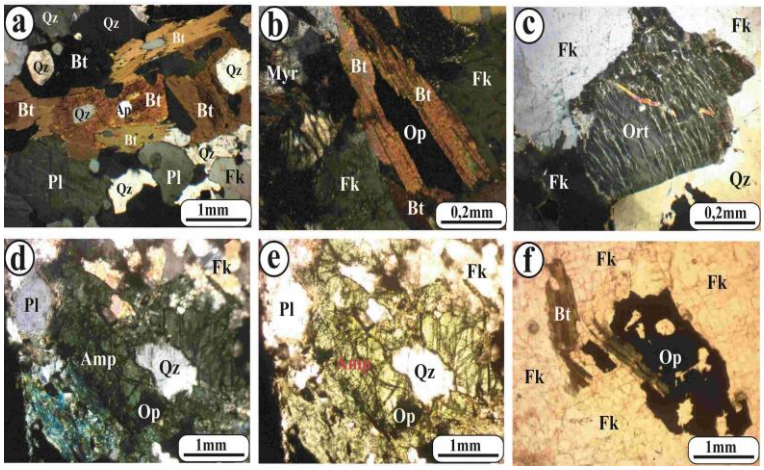


**Fig. 5:** Micrography of the Metamorphic Rock of Pamsi Locality. A) Grano-Lepidoblastic Texture of Orthogneiss (XPL); B) Biotite and Opaque Mineral Association (XPL); C) Perthitic Orthoclase (XPL); D) Granoblastic Texture of Amphibolite (XPL); E) Granoblastic Texture of Amphibolite (PPL); F) Opaque Mineral and Biotite Association (PPL).

## 4.2. Geochemistry

Chemical analyses of the rock sample are given in Table 1.

**Table 1:** Major (Wt%) and Trace Element Content (Ppm) in the Pamsi Rock

| Rock | Amphibole and biotite granite | | Leucogranite | | Granodiorite | Orthogneiss | Amphibolite |
|---|---|---|---|---|---|---|---|
| Sample | N51 | N52 | N31 | N11 | N13 | E41 | E02 |
| $SiO_2$ | 70.12 | 70.92 | 73.04 | 74.40 | 64.12 | 63.54 | 53.19 |
| $Al_2O_3$ | 14.76 | 14.66 | 14.98 | 14.18 | 14.51 | 14.24 | 13.98 |
| $Fe_2O_3$ | 2.84 | 1.95 | 0.65 | 0.58 | 4.01 | 4.83 | 12.83 |
| MgO | 1.66 | 1.71 | 0.12 | 0.28 | 2.61 | 3.94 | 3.78 |
| CaO | 1.72 | 1.52 | 1.21 | 1.18 | 6.52 | 4.12 | 5.61 |
| $Na_2O$ | 3.34 | 3.38 | 4.19 | 4.18 | 2.51 | 3.48 | 2.98 |
| $K_2O$ | 4.86 | 4.84 | 4.09 | 3.87 | 4.01 | 4.86 | 4.86 |
| $TiO_2$ | 0.06 | 0.07 | 0.88 | 0.49 | 0.64 | 0.56 | 2.16 |
| $P_2O_5$ | 0.08 | 0.08 | 0.06 | 0.07 | 0.08 | 0.09 | 0.09 |
| MnO | 0.04 | 0.04 | 0.06 | 0.05 | 0.02 | 0.03 | 0.03 |
| Total | 99.99 | 99.99 | 99.99 | 99.98 | 99.97 | 99.98 | 99.99 |
| Loi | 0.51 | 0.82 | 0.71 | 0.70 | 0.94 | 0.29 | 0.48 |
| $Na_2O+K_2O$ | 8.20 | 8.22 | 8.28 | 8.05 | 6.52 | 8.34 | 7.84 |
| $K_2O/Na_2O$ | 1.46 | 1.43 | 0.98 | 0.93 | 1.60 | 1.40 | 1.63 |
| A/NK | 1.06 | 1.08 | 1.11 | 1.07 | 0.71 | 0.77 | 0.69 |
| A/CNK | 1.37 | 1.36 | 1.32 | 1.28 | 1.71 | 1.29 | 1.37 |
| Cs | 8.80 | 1.40 | 5.90 | 11.30 | 1.60 | 1.20 | 4.60 |
| Rb | 99.00 | 114.00 | 108.00 | 93.00 | 111.00 | 82.00 | 133.00 |
| Ba | 814.00 | 1553.00 | 872.00 | 1053.00 | 1329.00 | 867.00 | 967.00 |
| Sr | 293.00 | 431.00 | 162.00 | 503.00 | 333.00 | 420.00 | 212.00 |
| Pb | 23.00 | 23.00 | 31.00 | 21.00 | 24.00 | 19.00 | 25.00 |
| Th | 30.70 | 4.30 | 33.20 | 18.80 | 22.60 | 7.60 | 245.70 |
| U | 9.90 | 0.60 | 35.40 | 11.30 | 1.00 | 1.20 | 4.00 |
| Zr | 480.00 | 820.00 | 713.00 | 405.00 | 423.00 | 1199.00 | 843.00 |
| Hf | 5.50 | 2.50 | 4.90 | 2.40 | 1.20 | 4.80 | 4.00 |
| Ta | 2.70 | 0.20 | 8.10 | 2.60 | 0.50 | 0.30 | 5.40 |
| Y | 27.00 | 19.00 | 31.00 | 15.00 | 20.00 | 15.00 | 30.00 |
| Nb | 33.00 | 16.00 | 32.00 | 12.00 | 10.00 | 16.00 | 22.00 |
| Sc | 8.80 | 1.40 | 5.90 | 11.30 | 1.60 | 1.20 | 4.60 |
| Cr | 106.00 | 112.00 | 43.00 | 86.00 | 67.00 | 55.00 | 65.00 |
| Ni | 50.00 | 28.00 | 25.00 | 46.00 | 39.00 | 17.00 | 25.00 |
| Co | 1.90 | 1.40 | 0.80 | 0.50 | 10.70 | 5.60 | 19.00 |
| V | 14.00 | 14.00 | 10.00 | 10.00 | 73.00 | 48.00 | 181.80 |
| W | 0.90 | 0.70 | 0.80 | 0.50 | 1.00 | 1.20 | 0.30 |
| Ga | 24.80 | 17.20 | 23.00 | 19.70 | 24.30 | 21.60 | 99.81 |
| Zn | 82.00 | 45.00 | 51.00 | 96.00 | 79.00 | 64.00 | 52.00 |
| Cu | 44.00 | 23.00 | 25.00 | 33.00 | 40.00 | 32.00 | 30.00 |
| La | 40.10 | 20.30 | 45.20 | 25.20 | 88.10 | 31.00 | 171.00 |
| Ce | 90.50 | 37.20 | 92.60 | 52.90 | 161.90 | 60.40 | 60.20 |
| Pr | 10.88 | 3.94 | 9.91 | 5.98 | 18.30 | 6.51 | 8.40 |
| Nd | 42.50 | 13.40 | 33.80 | 21.30 | 64.70 | 23.40 | 20.00 |
| Sm | 9.87 | 1.83 | 6.30 | 4.23 | 9.96 | 3.64 | 4.30 |
| Eu | 0.45 | 0.74 | 0.60 | 0.37 | 1.44 | 0.95 | 1.20 |
| Gd | 10.87 | 1.15 | 6.16 | 3.94 | 7.06 | 2.65 | 4.78 |
| Tb | 1.84 | 0.11 | 1.14 | 0.66 | 0.80 | 0.33 | 0.82 |
| Dy | 11.53 | 0.65 | 7.81 | 4.42 | 3.67 | 1.69 | 4.11 |
| Ho | 2.39 | 0.13 | 1.65 | 0.95 | 0.52 | 0.30 | 1.35 |
| Er | 7.32 | 0.40 | 5.57 | 3.19 | 1.16 | 0.88 | 4.33 |
| Tm | 0.96 | 0.05 | 0.80 | 0.49 | 0.14 | 0.11 | 0.60 |

| | | | | | | | |
|---|---|---|---|---|---|---|---|
| Yb | 6.00 | 0.44 | 5.67 | 3.40 | 0.86 | 0.81 | 3.56 |
| Lu | 0.80 | 0.06 | 0.77 | 0.50 | 0.12 | 0.11 | 0.72 |
| Ti | 357.54 | 417.13 | 5243.92 | 2919.91 | 3813.76 | 3337.04 | 12871.44 |
| (La/Yb)N | 4.54 | 31.34 | 5.42 | 5.03 | 69.59 | 26.00 | 32.63 |
| (Gd/Lu)N | 1.68 | 2.37 | 0.99 | 0.97 | 7.27 | 2.98 | 0.82 |
| Eu/Eu* | 0.13 | 1.56 | 0.29 | 0.28 | 0.52 | 0.93 | 13.07 |

#### 4.2.1. Determination of the nature of protholite of metamorphic rocks

The metamorphic rock samples plotted on the Werner [17] diagram (Fig. 6) confirm that the orthogneiss is ortho-derived and the amphibolite also has a magmatic origin. Because both metamorphic rocks have a magmatic protolith, they are discussed together with the granitoids.

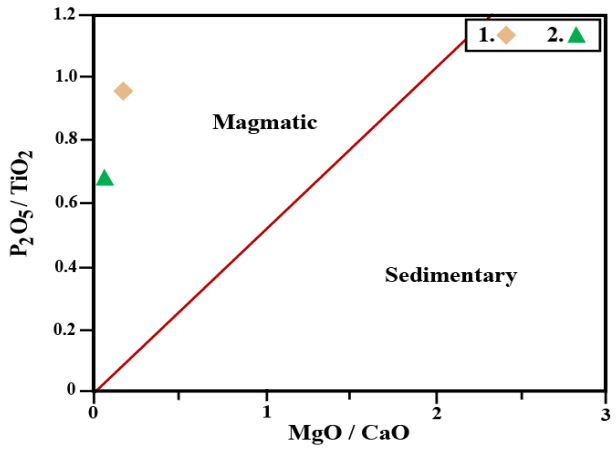


**Fig. 6:** Determination of the Nature of the Protolith of Rock from Pamsi Locality.

#### 4.2.2. Geochemical characterization

The rocks of the Pamsi region show the following oxide weight percentage ranges: 53.19–74.40% $SiO_2$; 13.98–14.98% $Al_2O_3$; 3.87–4.86% $K_2O$; 0.58–12.83% $Fe_2O_3$; 2.51–4.19% $Na_2O$; 1.18–5.61% CaO; 0.12–3.94% MgO; 0.06–2.16% $TiO_2$; and 0.06–0.09% $P_2O_5$. The sum of alkalis ($Na_2O + K_2O$) varies between 6.52 and 8.34%, and the $K_2O/Na_2O$ ratio varies between 0.92 and 1.63. Overall, the analyzed samples show medium Ba contents (814–1553 ppm), low Sr (162–503 ppm), and low Rb (82–133 ppm).

#### 4.2.3. Classification and nomenclature

The classification diagram of [18], adapted to plutonic rock by [19], allowed for the discrimination of samples from the study area (Fig. 7a). The rocks of the Pamsi locality form a suite ranging from syeno-diorite to granite through granodiorite. All rock samples fall within the sub-alkaline rock domain, except the orthogneiss sample, which is located in the alkaline rock field.
In the $K_2O$ versus $SiO_2$ diagram of [20] (Fig. 7b), the analyzed rock samples occupy the field of potassic and hyperpotassic calc-alkaline series and shoshonitic rocks.
The A/NK versus A/CNK diagram of [21] (Fig. 7c) indicates a molar ratio $Al_2O_3/(Na_2O+K_2O)$ or A/NK that varies between 1.28 and 1.71 and a molar ratio $Al_2O_3/(CaO+Na_2O+K_2O)$ or A/CNK that varies between 0.69 and 1.11. This diagram shows that the Pamsi rocks are predominantly peraluminous to metaluminous in nature, except the amphibolite sample, which falls in the hyperalkaline domain. All samples belong to the I-type granitoid domains.
In the FeOt/(MgO+FeOt) versus $SiO_2$ diagram of [22] (Fig. 7d), the rocks of our study area are predominantly magnesian except for two (02) samples (a leucogranite and the orthogneiss), which fall in the ferroan field.

#### 4.2.4. Majors and traces elements

In the [25] diagrams type major element variation (Fig. 8), the representative points of rocks from the Pamsi region show a decrease in $Al_2O_3$, $Fe_2O_3$, CaO, $TiO_2$, and $P_2O_5$ with increasing $SiO_2$ content. MgO, $Na_2O$, and $K_2O$ vary little and show no correlation with $SiO_2$.
The [25] diagrams of some trace elements versus silica (Fig. 9) show a dispersion of representative points of rock samples from the study area for Ba, Rb, Sr, Nb, Th, and Ni contents with increasing silica. The Zr-$SiO_2$ and V-$SiO_2$ diagrams show a linear regression with increasing $SiO_2$ content.

#### 4.2.5. Magmatic evolution (Rare Earth Elements (REE) and multielement)

The chondrite-normalized rare earth element (REE) spectra according to the values of [26] for rocks from the Pamsi region (Fig. 10a and 10c) are characterized by their high light rare earth element (LREE) content compared to heavy rare earth elements (HREE). The primitive mantle-normalized multi-element spectra (Fig. 10b and 10d) show their enrichment in LILE (Large Ion Lithophile Elements) compared to HFSE (High Field Strength Elements).

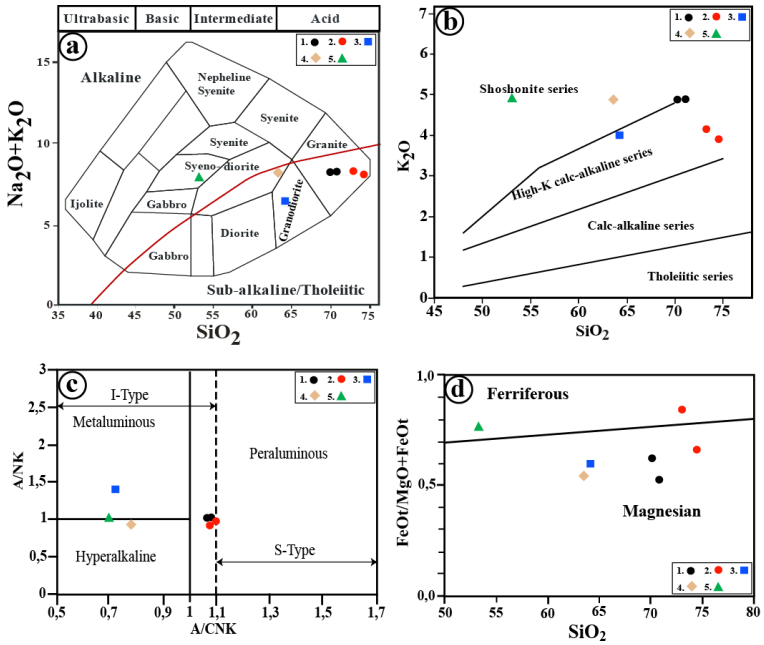


**Fig. 7:** A) Classification of Rocks from the Pamsi Locality in the Diagram of [18], Adapted to Plutonic Rock by [19]. The Bold Line Delimits the Alkaline and Sub-Alkaline Rock Fields. This Boundary Is From [23]; B) $K_2O$ Versus $Sio_2$ Diagram Allowing Discrimination of Rocks from the Locality. The Series Boundaries Are from [20]; C) Positions of Rocks from the Pamsi Locality in the Diagram Of [21]. A/NK = $Al_2O_3/(Na_2O+K_2O)$; A/CNK = $Al_2O_3/(Cao+Na_2O+K_2O)$ in Moles. The Boundaries Between I- and S-Type Granites Are from [24]; D) Position of Rocks from the Pamsi Locality in the Feot/(Mgo+Feot) Versus $Sio_2$ Diagram of [22] Frost Et Al. (2001), Showing the Ferroan and Magnesian Domains. 1. Amphibole-Biotite Granite; 2. Leucogranite; 3. Granodiorite; 4. Orthogneiss; 5. Amphibolite.

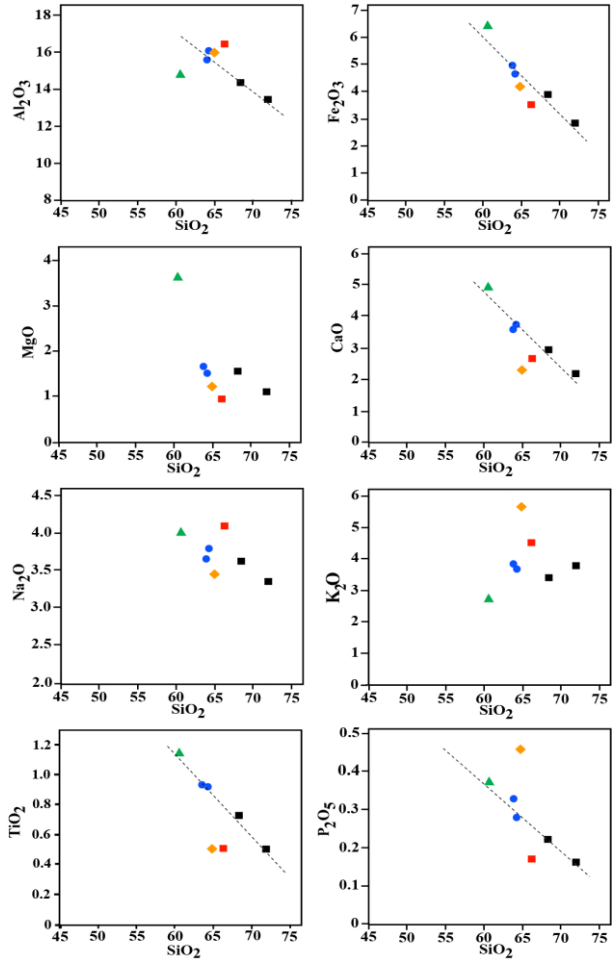


**Fig. 8:** [25] Diagram of Pamsi Rock, Showing the Variation of Oxides Versus SiO2. 1. Amphibole-Biotite Granite; 2. Leucogranite; 3. Granodiorite; 4. Orthogneiss; 5. Amphibolite.

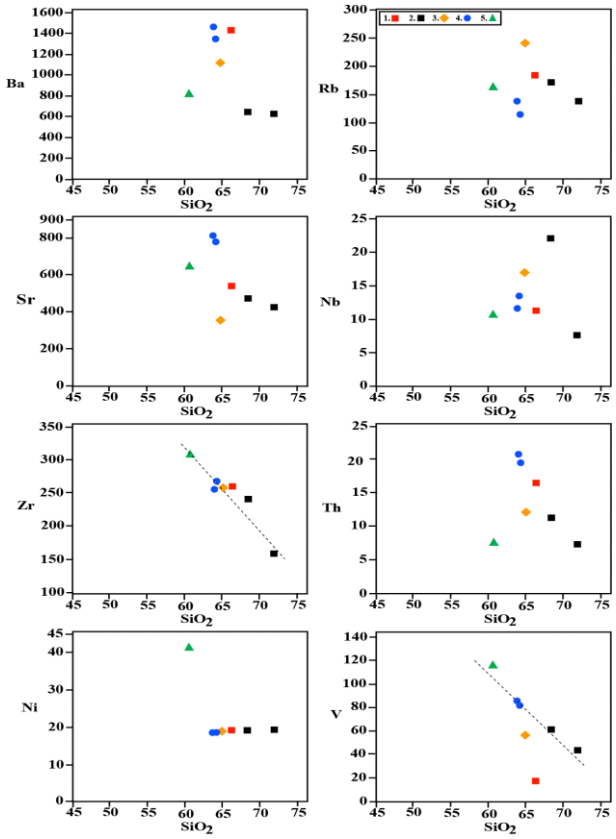


**Fig. 9:** [25] Diagram of Sum Trace Elements of Pamsi Rocks, Showing the Variation of the Trace Elements Versus $Sio_2$. 1. Amphibole-Biotite Granite; 2. Leucogranite; 3. Granodiorite; 4. Orthogneiss; 5. Amphibolite.

The REE spectra of plutonic rocks (Fig. 10a) show strong fractionation [(La/Yb)N = 4.54 – 69.59] and nearly flat profile segments for heavy rare earth elements (HREE) [(Gd/Lu)N = 0.97 – 7.27]. The samples show profiles with negative Eu anomaly (Eu/Eu* = 0.13 - 1.56), with the exception of one amphibole-biotite granite sample, which shows no Eu anomaly.
The analyzed plutonic rock samples from the study area show multi-element spectra profiles with negative anomalies in Ta, Sr, and Ti (Fig. 10b). These sample profiles show positive anomalies in U, Nb, Sr, and Zr.
The REE spectra of metamorphic rocks (Fig. 10c) show high fractionation [(La/Yb)N = 26.00 – 32.63] and nearly flat spectral segments for heavy rare earth elements [(Gd/Lu)N = 0.82 – 2.98]. No negative Eu anomaly is observed (Eu/Eu* = 0.93 – 13.07) for these two (02) analyzed samples.
The analyzed metamorphic rock samples from Pamsi show multi-element spectra profiles with negative anomalies in Ta, Nb, Sr, and Ti (Fig. 10d). These sample profiles show positive anomalies in Th, Zr, and Hf.

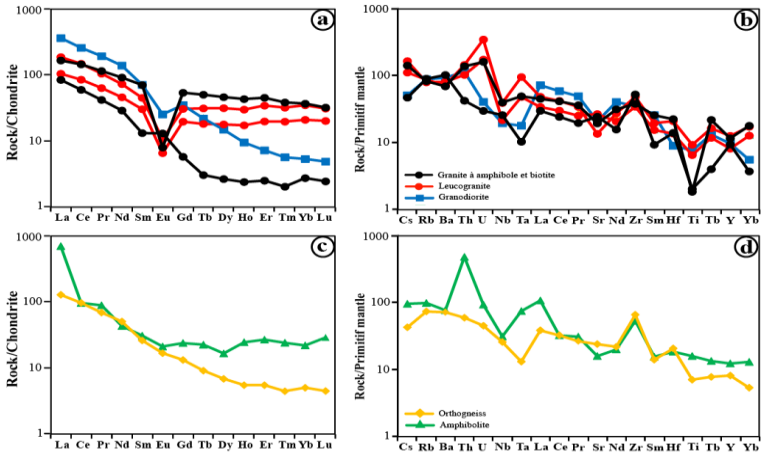


**Fig. 10:** Rare Earth Element Spectra (A and C); Multi-Element Spectra (B and D) of Rocks from the Pamsi Locality Normalized to the Values of [26].

## 5. Discussion

### 5.1. Petrography

The nomenclature of Pamsi rocks places the samples in the fields of granitoids ranging from syeno-diorite to granite (Fig. 7a). Based on textural relationships and mineral associations observed in thin sections, the crystallization sequence can be established as follows: oxide → apatite → amphibole → plagioclase → biotite → microcline → orthoclase → quartz. This sequence is typical of I-type granitoids and

reflects the progressive crystallization of a cooling magma under changing pressure-temperature conditions. Rocks with similar characteristics have been described in the Poli [4], Guider [9], Pitoa [10], and Kaélé [11] sectors of the North Cameroon Domain.

## 5.2. Geochemistry

The two metamorphic rock samples are ortho-derived (Fig. 6), indicating a magmatic protolith, and are therefore discussed alongside the plutonic rocks. The Pamsi rocks are characterized by hyperpotassic to shoshonitic calc-alkaline affinities (Fig. 7b), magnesian to slightly ferroan compositions (Fig. 7d), and metaluminous to peraluminous I-type signatures (Fig. 7c). Similar geochemical characteristics have been documented in the North Cameroon Domain at Poli [4], Guider [9], Pitoa [10], Kaélé [11], and Sinassi [27].

### 5.2.1. Petrogenesis

The REE patterns exhibit significant LREE enrichment relative to HREE, a characteristic feature of evolved granitic systems. The LREE enrichment reflects fractionation of accessory minerals such as apatite and monazite [28, 29], while HREE depletion is attributed to zircon fractionation during magmatic evolution. The negative Eu anomaly observed in most studied samples reflects plagioclase fractionation during parental magma evolution [30]. The absence of a negative Eu anomaly in one amphibole-biotite granite sample and in the two metamorphic samples can be explained by (1) limited incorporation of Eu into the plagioclase structure, (2) highly oxidizing conditions where Eu exists predominantly as $Eu^{3+}$ rather than $Eu^{2+}$, or (3) minimal plagioclase fractionation in the magma source [31]. Positive Eu anomalies in certain samples indicate plagioclase accumulation in the original magma [34]. The abundance of ferromagnesian minerals, particularly amphibole, suggests a significant mantle contribution to the magmatic source [35]. The overall parallelism of REE profiles indicates that these rocks are cogenetic and derived from a common parental magma [36 - 38].
Multi-element spider diagrams reveal pronounced negative Nb, Ta, and Ti anomalies, diagnostic of continental crust-derived magmas [39], [40]. The negative Ti anomaly indicates fractionation of Fe-Ti oxide minerals, consistent with the presence of opaque minerals in thin sections. Positive Zr and Ba anomalies further support a crustal signature. The metaluminous to peraluminous I-type character of the Pamsi granitoids, combined with their geochemical signatures, suggests derivation from a mixed magmatic source involving both continental crust and mantle components, similar to hybrid sources documented for metaluminous I-type granitoids in comparable tectonic settings [41], [42].

### 5.2.2. Geodynamic context

Tectonic discrimination diagrams provide insights into the geodynamic setting of granitoid emplacement. In the Nb vs. Y diagram of Pearce et al. [43] (Fig. 11a), most samples plot in the volcanic arc granitoid (VAG) to syn-collisional granitoid (Syn-COLG) field, indicating formation in a convergent tectonic setting. Two samples plot in the within-plate granitoid (WPG) field, suggesting possible post-collisional or extensional emplacement. In the Rb vs. (Y+Nb) diagram (Fig. 11b), samples predominantly occupy the VAG field, with the same two samples at the VAG–WPG boundary. This distribution indicates that the Pamsi granitoids were emplaced during the transition from active subduction to post-collisional extension, consistent with the late Pan-African orogenic evolution in the Central African Fold Belt (CAFB).

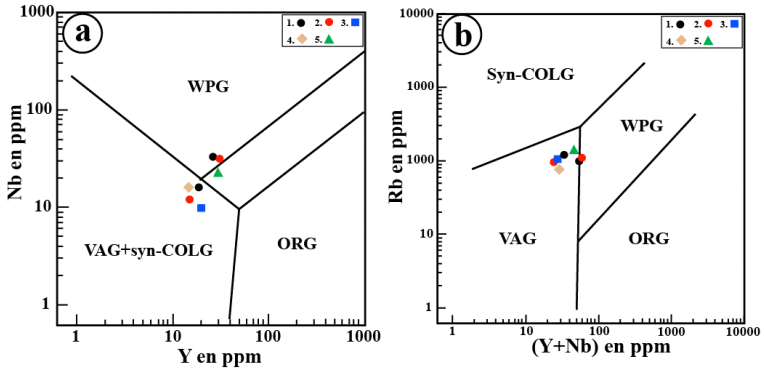


**Fig. 11:** A) Position of Rocks from the Pamsi Locality in the Tectonic Discrimination Diagram Y Versus Nb (In Ppm) of [43]; B) Position of Rocks in the Tectonic Discrimination Diagram Rb Versus (Y + Nb) Of [43]. (VAG + Syn-COLG: Volcanic Arc to Syn-Collisional Granitoids; VAG: Volcanic Arc Granitoids; WPG: within-Plate Granitoids; ORG: Ocean Ridge Granitoids). 1. Amphibole-Biotite Granite; 2. Leucogranite; 3. Granodiorite; 4. Orthogneiss; 5. Amphibolite.

### 5.2.3. Comparison with Panafrican granitoids from Cameroon

Comparative geochemical analysis reveals strong similarities between the Pamsi granitoids and other Pan-African plutonic rocks from the North Cameroon Domain. The granitoids from Guider [9], Pitoa [10], Mbip [32], Bafoussam [44], and Hangloa [45] display comparable geochemical signatures, including systematic negative Nb-Ta anomalies characteristic of subduction-related magmatism, negative Ti anomalies indicating Fe-Ti oxide fractionation, and positive Th anomalies. Regional variations in Sr behavior likely reflect differences in plagioclase fractionation intensity or source composition. The geochemical coherence among these granitoid suites confirms that they are products of the Pan-African orogenic cycle (ca. 630–580 Ma) in the CAFB [4, 10, 27]. The Pamsi granitoids are thus consistent with syn- to late-collisional magmatism associated with the assembly of Gondwana during Neoproterozoic to Early Paleozoic times [4, 10, 27].

## 5.3. Preliminary assessment of lithium exploration potential

The geochemical analysis of the seven rock samples reveals distinct pathfinder element signatures relevant to evaluating lithium exploration potential. It is important to emphasize that lithium was not directly measured in this study; all estimates presented below are indirect and preliminary, based on established geochemical correlations, and must be confirmed by direct analytical methods.

Samples N11 (amphibole-biotite granite) and N51 (amphibole-biotite granite) are distinguished by notable cesium enrichment, with Cs contents of 11.30 ppm and 8.80 ppm, respectively—values exceeding typical crustal reference values of 1–5 ppm [47]. These concentrations, combined with elevated Cs/Rb ratios (0.121 and 0.089, respectively), suggest an advanced degree of magmatic differentiation consistent with LCT-type granites (Lithium-Cesium-Tantalum) [48, 49]. Elevated tantalum (2.60–2.70 ppm) and uranium (9.90–11.30 ppm) in these same samples further suggest association with an evolved, possibly pegmatitic system [50].

Based on geochemical correlations between Cs and Li established for similar geological contexts [51], [52], and acknowledging the significant uncertainties inherent in such indirect estimates, the following preliminary lithium contents are proposed: N11: approximately 300–800 ppm Li; N51: approximately 200–500 ppm Li. Sample N31 (leucogranite), with a notably high tantalum content (8.10 ppm) and elevated uranium (35.40 ppm), also warrants attention as a secondary target, with an estimated Li content of approximately 150–400 ppm [53]. Several important limitations must be stated. First, the Cs-Li geochemical correlation is well-established for LCT pegmatite systems in general, but its quantitative application to the Pamsi rocks is uncertain without site-specific calibration. Second, no quantitative regression equation or calibration model was applied; the ranges given are order-of-magnitude estimates. Third, no direct mineralogical evidence (e.g., spodumene, lepidolite, or other Li-bearing minerals) has been documented at Pamsi. Consequently, the lithium values reported here should be treated solely as preliminary exploration indicators, not as resource estimates.

### 5.4. Metallogenic implications for exploration

The geochemical data from this study provide a basis for prioritizing future lithium exploration at Pamsi. Samples N11 and N51 exhibit geochemical signatures consistent with evolved LCT granites [48], making them the highest-priority targets for follow-up investigation. Sample N31 presents a distinct but potentially complementary geochemical signature. The Cs-Li correlation in LCT-type systems [51] supports using Cs and related pathfinder elements as first-order exploration guides, while recognizing that direct lithium analysis is essential before any economic significance can be attributed.

A preliminary ranking of exploration targets, based exclusively on indirect geochemical indicators, is as follows:

- N11: Highest-priority target; elevated Cs (11.30 ppm), high Cs/Rb ratio (0.121), elevated U; estimated Li 300–800 ppm (indirect, preliminary).
- N51: High-priority target; elevated Cs (8.80 ppm), high Cs/Rb ratio (0.089), elevated U; estimated Li 200–500 ppm (indirect, preliminary).
- N31: Secondary target; high Ta (8.10 ppm) and very high U (35.40 ppm); estimated Li 150–400 ppm (indirect, preliminary).

Recommended follow-up steps include: (1) direct lithium analysis of all samples, with priority on N11, N51, and N31; (2) systematic geological mapping and extended sampling to improve spatial representativeness; (3) mineralogical investigation (XRD, electron microprobe) to identify potential Li-bearing phases; and (4) prospection for associated pegmatite bodies in the field area. Comparison with well-documented LCT granite systems globally (e.g., Greenbushes, Australia; Bikita, Zimbabwe) would also help contextualize the Pamsi geochemical signatures and refine the exploration model.

## 6. Conclusion

This study presents the first integrated petrographic and geochemical characterization of granitoid and metamorphic rocks from the Pamsi locality in the North Cameroon Domain. The following principal conclusions are drawn: five main lithological units are identified, namely amphibole-biotite granite, leucogranite, granodiorite, orthogneiss, and amphibolite, all belonging to I-type, peraluminous to metaluminous, magnesian calc-alkaline granitoids; geochemical signatures characterized by strong LREE enrichment, negative Eu anomalies, and negative Ta-Nb and Ti anomalies indicate derivation from a mixed crustal-mantle magmatic source in a subduction to syn-collisional tectonic setting, consistent with the Pan-African orogenic cycle (ca. 630–580 Ma); the broader geodynamic context places the Pamsi granitoids within the syn- to late-collisional magmatism of the Central African Fold Belt, comparable to coeval suites across the North Cameroon Domain; indirect pathfinder element data, including elevated Cs, high Cs/Rb ratios, and elevated Ta and U in samples N11 and N51, suggest a preliminary exploration potential for lithium mineralization associated with evolved pegmatitic systems, although these indications remain provisional since lithium was not directly measured and all Li estimates are subject to significant uncertainty, thus requiring direct analytical confirmation and detailed mineralogical investigation before any resource-related conclusions can be drawn. This study provides a foundation for future lithium prospecting in the Pamsi area, with recommended priorities including direct Li analysis, particularly for samples N11, N51, and N31, extended systematic sampling, mineralogical identification of Li-bearing phases, and field prospection for associated pegmatite bodies, while comparison with global LCT pegmatite systems will help refine the local exploration model; more broadly, this work contributes to the understanding of the Pan-African metallogenic framework in Central Africa and highlights the region's potential as an underexplored critical mineral province.

## Acknowledgements

The authors thank the anonymous reviewers for their constructive comments and suggestions, which substantially improved the manuscript.

## Conflict of Interest

The authors declare that there is no conflict of interest related to this paper.

## References

[1] Kavanagh, L., Keohane, J., Garcia Cabellos, G., Lloyd, A., Cleary, J. (2018). Global Lithium Sources-Industrial Use and Future in the Electric Vehicle Industry: A Review. *Resources*, 7(3), 57. DOI: 10.3390/resources7030057.

[2] Kesler, S. E., Gruber, P. W., Medina, P. A., Keoleian, G. A., Everson, M. P., Wallington, T.J. (2012). Global lithium resources: Relative importance of pegmatite, brine, and other deposits. *Ore Geology Reviews*, 48, 55-69. https://doi.org/10.1016/j.oregeorev.2012.05.006.

[3] Bradley, D. C., McCauley, A. D., Stillings, L. M. (2017). Mineral-deposit model for lithium-cesium-tantalum pegmatites. *U.S. Geological Survey Scientific Investigations Report 2010-5070-O*, 48 p. https://doi.org/10.3133/sir20105070O.

[4] Toteu, S. F., Penaye J., Poudjom D. Y., (2004). Geodynamic evolution of the Pan-African belt in central Africa with special reference to Cameroon. *Canadian Jounal of Earth Sciences,* 41, 73-85. https://doi.org/10.1139/e03-079.

[5] Penaye, J., Kröner A., Toteu, S. F., Van Schmus, W. R., Tchakounte, J., Doumnang, J. C., (2006). Evolution of the Mayo Kebbi region as reveled by zircon dating: an early (ca. 740 Ma) Pan-African magmatic arc in southwestern Chad. *Journal of African Earth Sciences,* 44, 530-542. https://doi.org/10.1016/j.jafrearsci.2005.11.018.

[6] Ngako, V., Jegouzo, P., Nzenti, J. P., (1992). Champ de raccourcissement et de cratonisation du Nord-Cameroun du paléozoïque supérieur au paléozoïque moyen. *Comptes Rendus de l'Académie des Sciences*, *Paris,* 315, 457-463.

[7] Toteu, S. F., (1990). Geochemical characterization of the main petrographical and structural units of northern Cameroon: implications for Pan-African evolution. *Journal of African Earth Sciences*, 10, 615-624. https://doi.org/10.1016/0899-5362(90)90028-D.

[8] Penaye, J., (1988). Pétrologie et structure des ensembles métamorphiques au Sud-est de Poli (Nord Cameroun) : Rôles respectifs du socle protérozoïque inférieur et de l´accrétion crustale panafricaine. *Thèse de Doctorat, Université de Nancy I, France,* 196 p.

[9] Dawaï, D., Bouchez, J. L., Paquette, J. L., & Tchameni, R. (2013). The Pan-African quartz-syenite of Guider (north-Cameroon): Magnetic fabric and U-Pb dating of a late-orogenic emplacement. *Precambrian Research*, 236, 132-144. DOI: 10.1016/j.precamres.2013.07.008.

[10] Happi Djofna, C. R., Bouyo, M. H., Dawai, D., Tchameni, R., Kouedjou, L., Tchunte Fosso, M. P., Fotso Kengne, H.B. (2022). Contribution to the Petrogenesis of Pan-African Granitoids from East Pitoa in the Northern Cameroon Domain of the Central African Fold Belt: Implications for Their Sources and Geological Setting. *Journal of Geosciences and Geomatics*, 10(3), 112-125.

[11] Bello, B., Ganwa, A. A., Naimou, S., Simeni, W. A. N., Amadou, D. K., Yingyang, W. R., Haskandi, K. J. (2023). Structural Study of the Precambrian Basement of Kaele (Far North Cameroon): Contribution of Remote Sensing (Application of Landsat 8 OLI/TIRS Images) and Field Data. *Journal of Geosciences and Geomatics*, 11(1), 1-10. DOI: 10.12691/jgg-11-1-1.

[12] Toteu, S. F., Michard, A., Bertrand, J. M., Rocci, G., (1987). U-Pb dating of Precambrian rocks from northern Cameroon, orogenic evolution and chronology of the Pan-African belt of central Africa. *Precambrian Research,* 37, 71-87. https://doi.org/10.1016/0301-9268(87)90040-4.

[13] Ngako, V., Jegouzo, P., Nzenti, J. P., (1991). Le Cisaillement Centre Camerounais. Rôle structural et géodynamique dans l´orogenèse panafricaine. *Comptes Rendus de l'Académie des Sciences, Paris,* 313, 457-463.

[14] Nzenti, J. P., Ngako, V., Kombou, R., Penaye, J., Bassahak J., Njel, U. O., (1992). Structures régionales de la chaîne panafricaine au Nord-Cameroun. *Comptes Rendu de l'Académie des Sciences de Paris*, Tome 611, 115-119.

[15] Toteu, S. F, Yongue, F. R., Penaye J., Tchakounte, J., Ciriaque, S. A., Mouangue, Van Schmus, W. R., Deloule E., Stendal, H., (2006). U–Pb dating of plutonic rocks involved in the nappe tectonic in southern Cameroon: consequence for the Pan-African orogenic evolution of the central African fold belt. *Journal of African Earth Sciences,* 44. 479-493. https://doi.org/10.1016/j.jafrearsci.2005.11.015.

[16] Bouyo, H. M., Toteu, S. F., Deloule, E., Penaye, J., Van Schmus, W. R., (2009). U-Pb and Sm-Nd dating of high-pressure granulites from Tcholliré and Banyo regions: Evidence for a Pan-African granulite facies metamorphism in north-central Cameroon. *Jounal of African Earth Science,* 54, 144-154. https://doi.org/10.1016/j.jafrearsci.2009.03.013.

[17] Werner, C. D., (1987). Saxonian granulitee: A contribution to the geological diagnosis of origine rocks in high-metam orphic complexes. Gerlands Beitraege zur Geophisik, 96, 271-290.

[18] Cox, K. G., Bell, J. D., Pankust, R. J., (1979). The interpretation of igneous rocks. *George Allen & Unwin.* https://doi.org/10.1007/978-94-017-3373-1.

[19] Wilson, M., (1989). Igneous Petrogenesis. *London: Unwin Hyman*, *London,* 466p. https://doi.org/10.1007/978-1-4020-6788-4.

[20] Le Maitre, R. W., (1989). A Classification of Igneous Rocks and Glossary of Terms. Recommendations of the IUGS Commission on the Systematics of Igneous Rocks. *Oxford: Blackwell.* 193p.

[21] Maniar, P. D., Piccoli, P. M., (1989). Tectonic Discrimination of Granitoids. *The Geological Society of America,* 101, 635-643. https://doi.org/10.1130/0016-7606(1989)101<0635:TDOG>2.3.CO;2.

[22] Frost, B. R., Barnes, C. G., Collins, W. J., Arculus, R. J., Ellis, D. J., Frost, C. D., (2001). A geochemical classification for granitic rocks. *Journal of Petrology,* 42, 2033-2048. https://doi.org/10.1093/petrology/42.11.2033.

[23] Irvine, T. N., Barragar, W. R. A., (1971). A guide to the chemical classification of the common volcanic rocks. *Canadian Journal of Earth Sciences,* 8, 523-548. https://doi.org/10.1139/e71-055.

[24] Chappell, B. W., White, A. J. R., (1992). I- and S-Type Granites in the Lachlan Fold Belt. *Transactions of the Royal Society of Edinburgh*: *Earth Sciences,* 83, 1-26. https://doi.org/10.1130/SPE272-p1.

[25] Harker, (1909). The natural history of igneous rocks. *Methuen, London.* https://doi.org/10.2307/1777000.

[26] Mc Donough, W. F., Sun, S. S. (1995). The composition of the Earth. *Chemical Geology,* 120, 223-253. https://doi.org/10.1016/0009-2541(94)00140-4.

[27] Bouyo, H. M., Penaye, J., Njel, U. O., Moussango, I. A. P., Sep, N. J. P., Nyama, A. B., Wassouo, W. J., Abate, E. J. M., Yaya, F., Mahamat, A., Hao, Y., Fei, W., (2016). Geoochrological, Geochemical and Mineralogical Contraints of Emplacement Depth of TTG suite from the Sinassi Batholith in the Central African Fold Belt (CAFB) of Northern Cameroon: Implications for Tectonomagmatic Evolution. Journal of African Earth Science, 116, 9-41. https://doi.org/10.1016/j.jafrearsci.2015.12.005.

[28] Rollinson, H. R. (1993). Using Geochemical Data: Evaluation, Presentation, Interpretation. *Longman Scientific & Technical,* 352 p.

[29] Zaraisky, G., Aksyuk, A., Devyatova, V., Udoratina, O., Chevychelov, V., (2009). The Zr/Hf ratio as a fractionation indicator of rare-metal granites. *Petrology,* 17(1), 25-45. https://doi.org/10.1134/S0869591109010020.

[30] Zhu, D., Mo, X., Wang, L., Zhao, Z., Niu, Y., Zhou, C., Yang, Y., (2009). Petrogenesis of highly fractionated I-type granites in the Zayu area of eastern Gangdese, Tibet: Constraints from zircon U-Pb geochronology, geochemistry and Sr-Nd-Hf isotopes. *Science in China, Series D: Earth Sciences,* 52(9), 1223-1239. https://doi.org/10.1007/s11430-009-0132-x.

[31] Davidson, J. P., McMillan, N. J., Moorbath, S., Worner, G., Harmon, R. S., Lopez-Escobar, L., (1990). The Nevados de Payachata volcanic region (18°S/69°W, N) II. Evidence for widespread crustal involvement in Andean magmatism. *Contributions to Mineralogy and Petrology,* 105, 412-432. https://doi.org/10.1007/BF00286829.

[32] Nomo, N. E., Tchameni, R., Vanderhaeghe, O., Barbey, P., Fosso, T. P. M., Wambo, T. J. D., Lemdjou, B. Y., Saha, A. N., (2015). Petrography and Geochemistry of the Mbip granitic massif, SW Tcholiré (Central North Cameroon): Petrogenetic and geodynamic implication. *International Journal of Geosciences,* 6, 761-775. https://doi.org/10.4236/ijg.2015.67062.

[33] Amadou, D. K., Naimou, S., Ntoumbé, M., Amaya, A. A. D., Bello, B., Haskandi, K. J., Awé, W. S., Ngounouno, I., (2021). Petrographic and geochemical study of Doua granitoids (Adamawa-Yadé domain, center Cameroon): Petrogenesis and geodynamic implication. *International Journal of Advenced Geosciences*, 9 (2), 99-109. https://doi.org/10.14419/ijag.v9i2.31702.

[34] Bau, M., 1991. Rare-earth element mobility during hyrothermal and metamorphic fluid-rock interaction and significance of the oxidation sate of europium. Chemical Geology, 93 (3-4), 219-230. https://doi.org/10.1016/0009-2541(91)90115-8.

[35] Peycru, P., Dupin, J. M., Fogelgesang, J. F., Van, D. R. C., Cariou, F., Perrier, C., Augère, B., (2008). *Géologie, Tout-En-Un. BCPST. Dunod, Paris,* 641 p.

[36] Heinhorst, J., Lehmann B., Seltmann, S., (1996). New geological data on granitic rocks of central Kazakhstan. In Granite-related ore deposits of central Kazakhstan and adjacent areas (eds. V. Shatov, R. Selmann, A. Kremenetssky, B. Lehmann, V. Popov, and P. Ermolov). *Glagol publishing House, St. Petersburg.*

[37] Zoheir, B. A., Mehanna, A. M., Qaoud, N. N., (2008). Geochemistry and geothermobarometry of the Um Eleiga Neoproterozoic island arc intrusive complex, SE Egypt: genesis of a potential gold-hosting intrusion. *Applied Earth Sciences: IMM Transactions section B,* 117(3), 89-111. https://doi.org/10.1179/174327508X375620.

[38] Robin, G., (2010). Ignous rock and processes: A pratical guide. Wiley-Blackwell, Eedition print 2010, 428p.

[39] Taylor, S. R., McLennan, S. M., (1985). The continental cust: its composition and evolution. *Blackwell,* 312p.

[40] Rudnick, R. L., Fountain, D. M., (1995). Nature and composition of the Continental-Crust a Lower Crust perspective. *Revue of Geophysics,* 33(3), 267-309. https://doi.org/10.1029/95RG01302
[41] Scoates, J. S., Frost, C. D., Mitchell, J. N., Lindsley, D. H., Frost, B. R., (1996). Residual liquid origin for a monzonite intrusion in a mid-Proterozoic anorthosite complex: The Sybille intrusion, Laramie anorthosite complex, Wyoming. *Geological Society of America Bulletin,* 108, 1357-1371. https://doi.org/10.1130/0016-7606(1996)108<1357:RLOFAM>2.3.CO;2.
[42] Anderson, I. C., Frost, C. D., Frost, B. R., (2003). Petrogenesis of the Red Mountain pluton, Laramie anorthosite complex, Wyoming: implications for the origin of A-type granites. In: Medaris, L. G. Jr, Byers, C. W., Mickelson, D. M. & Shanks, W. C. (eds). Proterozoic geology: selected papers from an international symposium, *Precambrian Research,* 124, 243-267. https://doi.org/10.1016/S0301-9268(03)00088-3.
[43] Pearce, J. A., Harris, N. B. W., Tindle, A. G. (1984). Trace element discrimination diagrams for the tectonic interpretation of granitic rocks. *Journal of Petrology*, 25(4), 956-983. https://doi.org/10.1093/petrology/25.4.956.
[44] Djouka-Fonkwé, M. L., Schulz, B., Schüssler U., Tchouankoué, J. P., Nzolang, C., 2008. Geochemistry of the Bafoussam Pan-African I- and S-type granitoids in western Cameroon. *Journal of African Earth Sciences,* 50, 148-167. https://doi.org/10.1016/j.jafrearsci.2007.09.015.
[45] Yaya, F., Mero Y., Tchameni, R., Wassouo, W. J., Amadou, D. K., Penaye, J., Mahamat, A., Nomo, N. E. (2022). Peraluminous granitoids within the Hangloa area, Adamawa-Yadé Domain, Cameroon: Petrogenesis and tectonic implication. *Acta Geochimica,* pp. 1-17.
[46] Abdelsalam, M. G., Liégeois, J. P., Stern, R.J. (2002). The Saharan Metacraton. *Journal of African Earth Sciences*, 34(3-4), 119-136. https://doi.org/10.1016/S0899-5362(02)00013-1.
[47] Rudnick, R. L., and Gao, S. (2003). Composition of the continental crust. *Treatise on Geochemistry*, 3, 1-64. https://doi.org/10.1016/B0-08-043751-6/03016-4.
[48] Cerny, P., Blevin, P. L., Cuney, M., Breaks, F. W. (2005). Granite-related ore deposits. *Economic Geology 100th Anniversary Volume*, 337-370. https://doi.org/10.5382/AV100.12.
[49] Linnen, R. L., Van Lichtervelde, M., Cerny, P. (2012). Granitic pegmatites as sources of strategic metals. *Elements*, 8(4), 275-280.
[50] London, D. (2008). Pegmatites. *The Canadian Mineralogist*, Special Publication 10, 347 p. https://doi.org/10.2113/gselements.8.4.275.
[51] Tischendorf, G., Förster, H. J., Gottesmann, B., Rieder, M. (1997). On Li-bearing micas: estimating Li from electron microprobe analyses and an improved diagram for graphical representation. *Mineralogical Magazine*, 61(409), 809-834. https://doi.org/10.1180/minmag.1997.061.409.05.
[52] Bowell, R. J., Lagos, L., De los Hoyos, C. R., Declercq, J. (2020). Classification and characteristics of natural lithium resources. *Elements*, 16(4), 259-264. https://doi.org/10.2138/gselements.16.4.259.
[53] Ballouard, C., Poujol, M., Boulvais, P., Branquet, Y., Tartèse, R., Vigneresse, J. L. (2016). Nb-Ta fractionation in peraluminous granites: A marker of the magmatic-hydrothermal transition. *Geology*, 44(3), 231-234. https://doi.org/10.1130/G37475.1.